Supporting Information

Trends and Descriptors of Heterogeneous Hydroformylation Activity and Selectivity of RhM_3 (M = Fe, Co, Ni, Cu and Zn) Catalysts

Zhongtian Mao,[a†] Haoyue Guo,[a†] Zhenhua Xie,[a,b,*] Ping Liu[a,*] and Jingguang G. Chen[a,b,*]

[a] *Chemistry Division, Brookhaven National Laboratory, Upton, NY 11973.*
[b] *Department of Chemical Engineering, Columbia University, New York, NY 10027.*

1. Methods

1.1. Experimental Methods

The Rh/MCM-41 and RhM_3/MCM-41 catalysts were synthesized with an incipient wetness co-impregnation method. The metal precursors ($Rh(NO_3)_3 \cdot xH_2O$, $Fe(NO_3)_3 \cdot 6H_2O$, $Co(NO_3)_2 \cdot 6H_2O$, $Ni(NO_3)_2 \cdot 6H_2O$, $Cu(NO_3)_2 \cdot 3H_2O$, $Zn(NO_3)_2 \cdot 6H_2O$) and the supports MCM-41 (hexagonal, 0.98 cm^3/g pore volume, 2.1-2.7 nm pore size, ~1000 m^2/g) were purchased from Sigma Aldrich. The loading amounts (wt%) were 1.00% for Rh and 1.73% for the secondary metal M (M = Fe, Co, Ni, Cu, Zn) corresponding to an atomic ratio of Rh:M = 1:3. The aqueous solution of metal precursors was mixed with the MCM-41 support, followed by stirring and drying at 50 °C overnight. The dried catalysts were then calcined at 290 °C for 2 h with a heating rate of 0.8 $°C \cdot min^{-1}$.

Pulse CO chemisorption experiments were performed in AMI-300ip (Altamira) instrument. In a U-shape quartz tube, about 50 mg catalyst was first pretreated under He atmosphere at 120 °C for 30 min and then cooled down to 35 °C. The catalyst was then exposed to a mixture of H_2/Ar = 5/45 $mL \cdot min^{-1}$, heated up to 200 °C at a ramping rate of 10 $°C \cdot min^{-1}$, and held for 1 h. After reduction, the catalyst was cooled to 35 °C again, and 10% CO in He was pulsed into the quartz tube. The number of active sites on the catalyst can be estimated by the amount of chemisorbed CO molecules.

The performance of the synthesized catalysts was evaluated in a quartz tube flow reactor under ambient pressure. 200 mg of the catalyst (60-80 mesh) was loaded in the flow reactor. The catalyst bed was first heated to 200 °C in N_2 atmosphere, and subsequently exposed to the reaction stream of $C_2H_4/H_2/CO/N_2$ = 3/3/3/3 $mL \cdot min^{-1}$. The products at the outlet of the reactor were analyzed with an Agilent 7890B gas chromatography (PLOT Q and MOLESEIVE columns) equipped with a thermal conductivity detector and a flame ionized detector. The relative response factor (RRF) of calibration for C_2H_6 was obtained relative to the internal standard N_2. All the other hydrocarbon species were calibrated based on their effective carbon numbers[1] ($ECN_{C2H4\ or\ C2H6}$ = 2, $ECN_{C3H6\ or\ C3H8}$ = 3, ECN_{C3H6O} = 2, ECN_{C3H8O} = 2.4) and the RRF of C_2H_6. The elemental balance of carbon was 100±4%. The conversion of C_2H_4 (X), and the yield of product i (Y_i) was calculated as:

$$X = \frac{\left[F_{C_2H_4}\right]_{in} - \left[F_{C_2H_4}\right]_{out}}{\left[F_{C_2H_4}\right]_{in}} \times 100\% \ ,$$

$$Y_i = \frac{\left[F_i\right]_{out}}{\left[F_{C_2H_4}\right]_{in}} \times 100\% \ ,$$

where $[F_{C2H4}]_{in}$ and $[F_{C2H4}]_{out}$ refer to the inlet and outlet molar flow rate of C_2H_4, and $[F_i]_{out}$ refers to the outlet molar flow rate of product *i*. The turnover frequency (TOF) of C_2H_4 conversion was calculated using the flow rate of converted C_2H_4, $[F_{C2H4}]_{in} - [F_{C2H4}]_{out}$, the mass of the catalyst m_{cat} (200 mg), and the CO uptake:

$$TOF = \frac{\left[F_{C_2H_4}\right]_{in} - \left[F_{C_2H_4}\right]_{out}}{\left(CO\ uptake\right) \times m_{cat}} .$$

To compare the selectivity of the catalysts, Rh/MCM-41 and RhM_3/MCM-41 (M = Co, Ni, Cu) were diluted with the support material MCM-41 to achieve comparable C_2H_4 conversion to $RhFe_3$/MCM-41. The C_2H_4 conversion on $RhZn_3$/MCM-41 was much lower than other catalysts. Thus, the loading of $RhZn_3$/MCM-41 was increased from 200 mg to 400 mg. The procedure of the flow reactor test is the same as described above. The selectivity of product *i* (S_i) is calculated as:

$$S_i = \frac{\left[F_i\right]_{out}}{\left[F_{C_2H_4}\right]_{in} - \left[F_{C_2H_4}\right]_{out}} \times 100\% \ .$$

1.2. Computational Methods

Spin-polarized DFT calculations were performed with the projector-augmented-wave (PAW) approach[2,3] and the generalized gradient approximation (GGA) exchange-correlation functional by Perdew, Burke and Ernzerhof (PBE)[3] as implemented in the *Vienna Ab Initio Simulation Package* (VASP).[2,5] The kinetic energy cutoff for the plane wave basis of 400 eV was employed. The Methfessel-Paxton order I method was used to describe the Fermi-distribution of electronic states in the metallic systems with an artificial electronic temperature of k_BT = 0.2 eV. The total energy was converged better than 10^{-7} eV/atom, and the Hellman-Feynman force on each atom was less than 0.03 eV/Å. The first Brillouin zone was sampled on a Γ-centered 3 × 3 × 1 *k*-mesh. A Hubbard U correction of U_{eff} = 5 eV was applied to Fe d orbitals based on previous literature.[6]

The Rh(111) surface was modeled using a 4-layer 4 × 4 surface slab. To determine the surface configurations of RhM_3 (M = Fe, Co, Ni, Cu, Zn) bimetallic catalysts, three slab models were considered following a similar approach in previous literature:[7] the bulk-terminated surface to describe the stoichiometric mixed alloy RhM_3(111), the skin Rh/M(111) or the sandwich M/Rh/M(111) model to simulate the two extreme cases of surface segregation. In addition, the configurations under activation of CO, hydrogen, and ethylene, were also considered by saturate adsorption of a layer of *CO on top of the three types of alloy surfaces. Although mild reaction conditions are expected, the formation of oxide-metal interfaces is also likely when the secondary metal can be easily oxidized, *e.g.*, Fe and Zn. Indeed, in the results part, we observed that for $RhFe_3$ and $RhZn_3$, the oxide-metal interfaces provide better

prediction for the selectivity, rather than the bulk-terminated surfaces. The most preferred configuration for RhM_3 under reaction conditions was selected for the potential energy diagram calculations. Therefore, the bulk-terminated $RhCo_3$(111) and $RhNi_3$(111) of 4-layer 4 × 4 slab was constructed using a L_{12} cubic crystal structure following previous literatures.[8] The skin model of Rh/Cu(111) of 4-layer 4 × 4 slab was constructed to describe the segregated $RhCu_3$ surface. The active phase of $RhFe_3$ and $RhZn_3$ surfaces under reaction conditions were modeled using Fe_3O_4/Rh(111) and Zn_3O_4/Rh(111), respectively, by depositing a small MO_x (M = Fe, Zn) cluster on a 4-layer 5 × 5 Rh(111) surface to account for the formation of metal/oxide interfaces due to the strong binding between Fe/Zn and oxygenate species. The size of the cluster was determined using a previous reported approach,[7,9] and the formation energies of MO_x cluster on Rh(111) surface were calculated referenced to Rh(111) surface, metallic M and gaseous oxygen. A 20 Å thick vacuum was added along the perpendicular direction to avoid the interactions between the slabs. During geometry optimization, the bottom two layers are fixed at the bulk positions while the rest layers were allowed to relax. Dipole corrections were added to compensate for the artificial charge polarization between the top and bottom surfaces.

The binding energy of an adsorbate is calculated as

$$BE = E_{\text{adsorbate/slab}} - E_{\text{slab}} - E_{\text{adsorbate}}$$

where $E_{\text{adsorbate/slab}}$, E_{slab} and $E_{\text{adsorbate}}$ are the DFT total energies of slab with the adsorbate, bare slab and the adsorbate species in the gas phase, respectively. According to the previous study,[10] the error for DFT-calculated binding energy using PBE functionals on metal surfaces is typically within 0.2 eV. While the difference in binding from one catalyst to the next, which is the focus of current study, can cancel some of system errors and describe the experimentally measured trend more accurately as shown in our previous studies.[11,12]

The reaction energy of a step is calculated as

$$\Delta E = E_{\text{products}} - E_{\text{reactants}}$$

where E_{products} and $E_{\text{reactants}}$ are the summation DFT total energies of products and reactants for a certain reaction step, respectively.

2. DFT Results

Table S1. The DFT total energy energies for three configurations considered over bare and CO-saturated surface on (111) facet of RhM_3 (M = Co, Ni, Cu).

Composition	**Bare (111) surface**	
	Configuration	E_{total} **(eV)**
$RhCo_3$	mix	-107.74
	sandwich	-104.53
	skin	-106.99
$RhNi_3$	mix	-89.36
	sandwich	-88.14
	skin	-88.65
$RhCu_3$	mix	-69.48
	sandwich	-68.64
	skin	-68.39

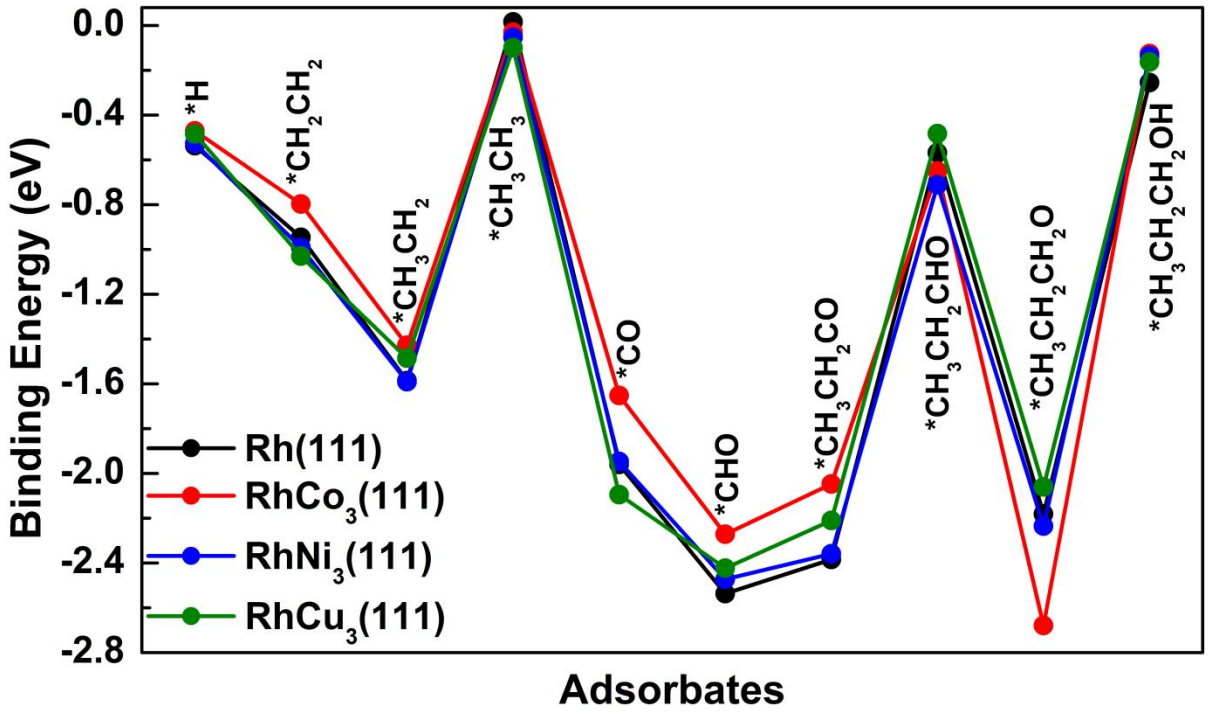

Fig. S1 Binding energies of the intermediates over Rh(111), $RhCo_3$(111), $RhNi_3$(111) and $RhCu_3$(111) surfaces.

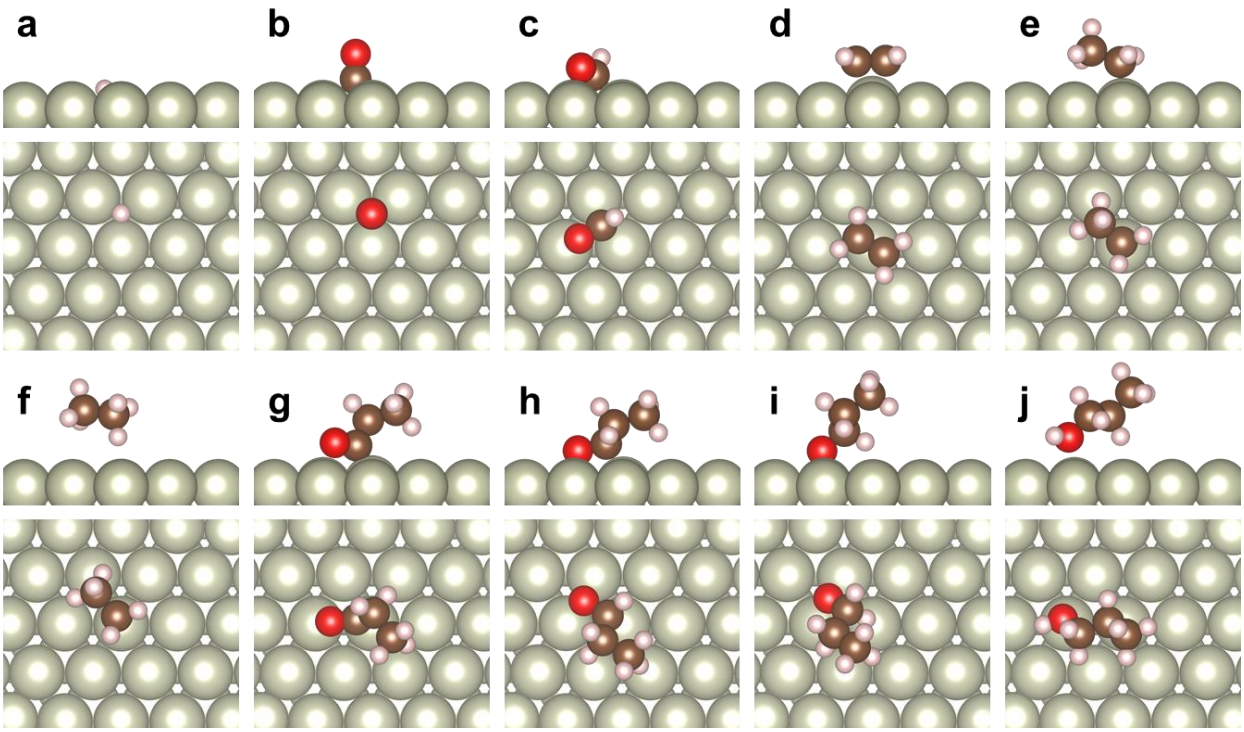

Fig. S2 The DFT-optimized geometries of the intermediates over Rh(111) surface. Top image (side view) and bottom image (top view) of (a) *H, (b) *CO, (c) *CHO, (d) *CH_2CH_2, (e) *CH_3CH_2, (f) *CH_3CH_3, (g) *CH_3CH_2CO, (h) *CH_3CH_2CHO, (i) *$CH_3CH_2CH_2O$, (j) *$CH_3CH_2CH_2OH$. (H: white; C: brown; O: red; Rh: cream).

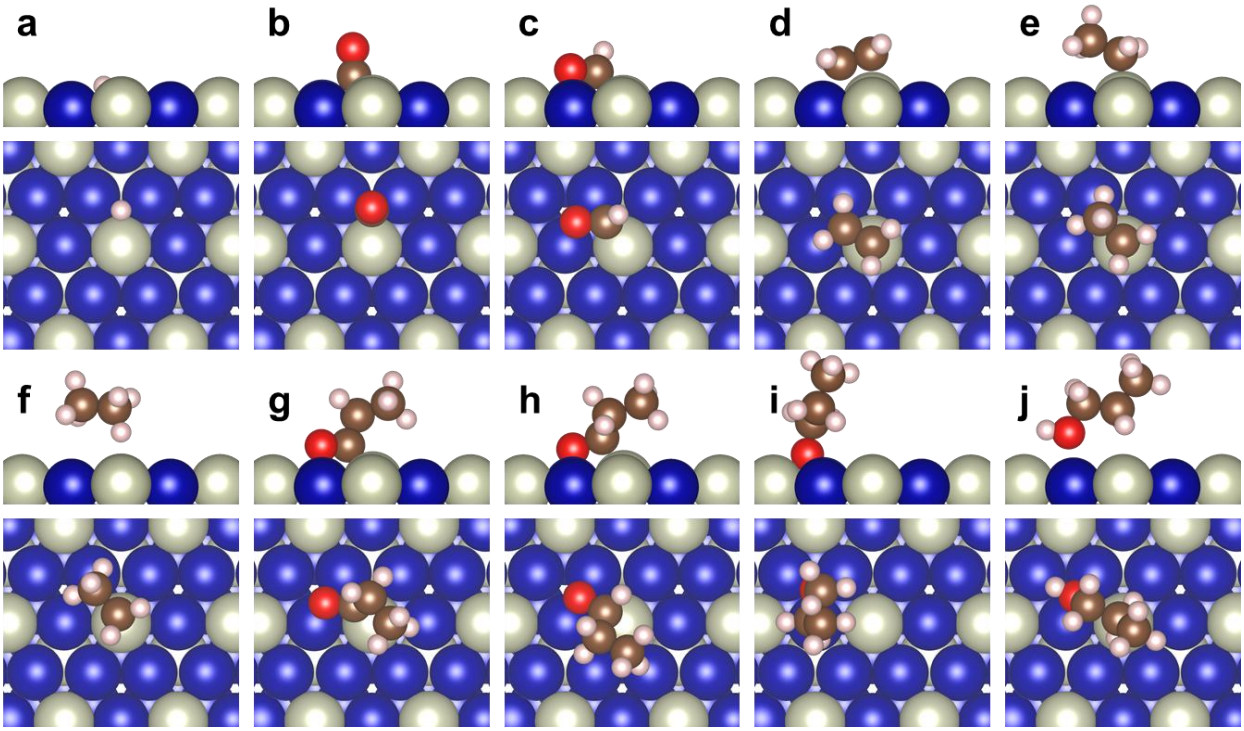

Fig. S3 The DFT-optimized geometries of the intermediates over $RhCo_3(111)$ surface. Top image (side view) and bottom image (top view) of (a) *H, (b) *CO, (c) *CHO, (d) $*CH_2CH_2$, (e) $*CH_3CH_2$, (f) $*CH_3CH_3$, (g) $*CH_3CH_2CO$, (h) $*CH_3CH_2CHO$, (i) $*CH_3CH_2CH_2O$, (j) $*CH_3CH_2CH_2OH$. (H: white; C: brown; O: red; Rh: cream; Co: blue).

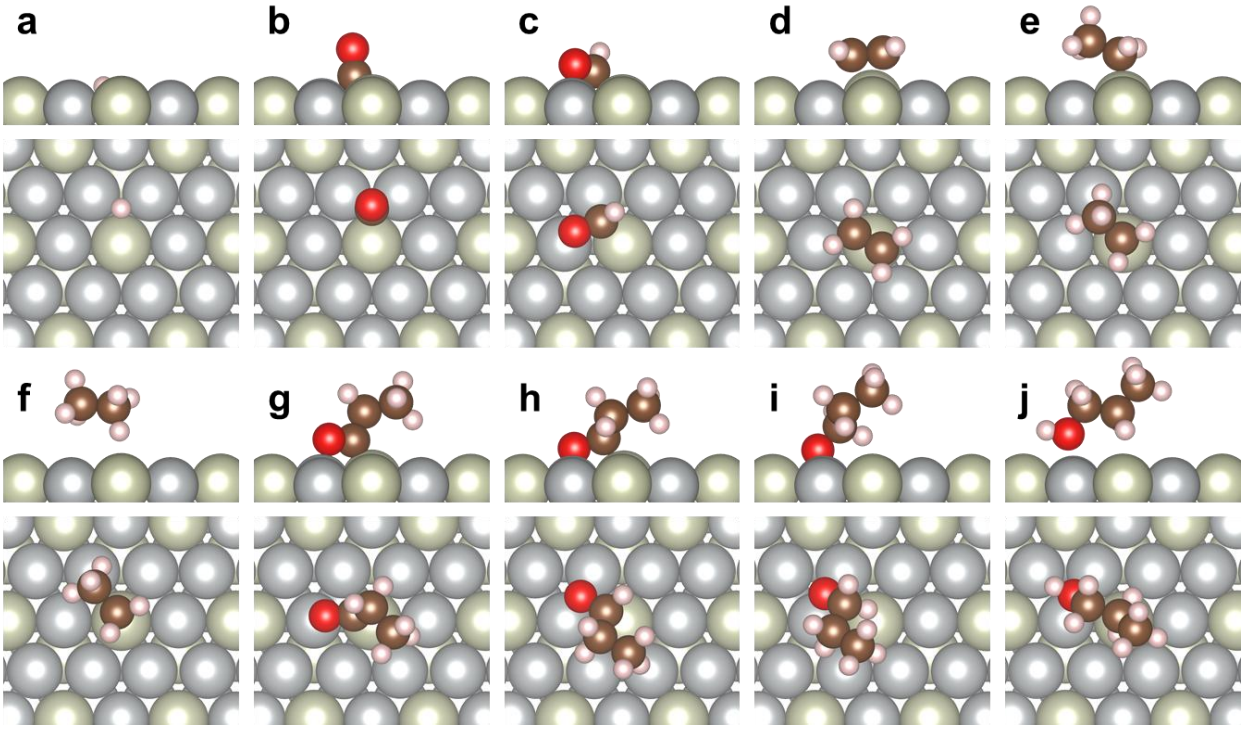

Fig. S4 The DFT-optimized geometries of the intermediates over $RhNi_3(111)$ surface. Top image (side view) and bottom image (top view) of (a) *H, (b) *CO, (c) *CHO, (d) $*CH_2CH_2$, (e) $*CH_3CH_2$, (f) $*CH_3CH_3$, (g) $*CH_3CH_2CO$, (h) $*CH_3CH_2CHO$, (i) $*CH_3CH_2CH_2O$, (j) $*CH_3CH_2CH_2OH$. (H: white; C: brown; O: red; Rh: cream; Ni: silver).

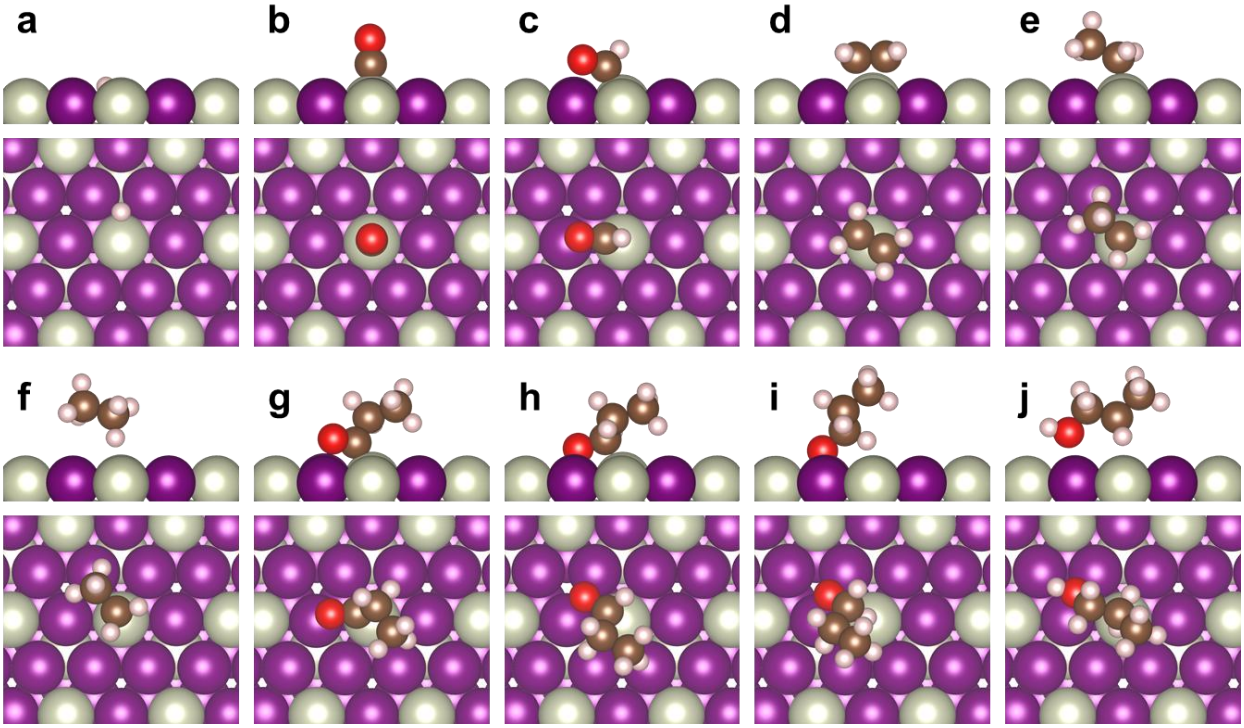

Fig. S5 The DFT-optimized geometries of the intermediates over $RhCu_3(111)$ surface. Top image (side view) and bottom image (top view) of (a) *H, (b) *CO, (c) *CHO, (d) $*CH_2CH_2$, (e) $*CH_3CH_2$, (f) $*CH_3CH_3$, (g) $*CH_3CH_2CO$, (h) $*CH_3CH_2CHO$, (i) $*CH_3CH_2CH_2O$, (j) $*CH_3CH_2CH_2OH$. (H: white; C: brown; O: red; Rh: cream; Cu: purple).

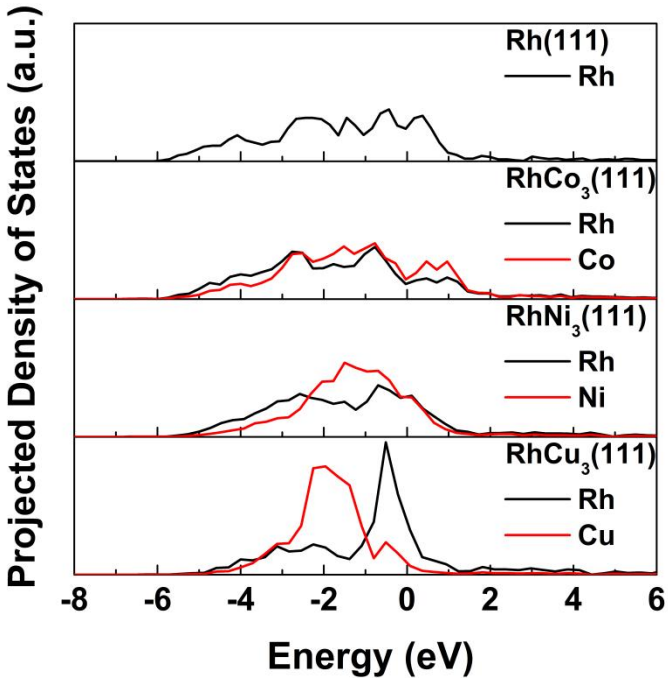

Fig. S6 Projected density of states (PDOS) for surface metal atoms over bare Rh(111), $RhCo_3$(111), $RhNi_3$(111) and $RhCu_3$(111) surfaces, where the energy was calibrated with respect to the Fermi-level.

3. References

1. F. Benjamin, Z. L. Xie, A. Trunschke. *Chem. Ing. Tech.*, 2013, **85**, 1290-1293.
2. G. Kresse and D. Joubert, *Phys. Rev. B*, 1999, **59**, 1758–1775.
3. P. E. Blöchl, *Phys. Rev. B*, 1994, **50**, 17953–17979.
4. J. P. Perdew, K. Burke and M. Ernzerhof, *Phys. Rev. Lett.*, 1996, **77**, 3865–3868.
5. G. Kresse and J. Furthmüller, *Phys. Rev. B*, 1996, **54**, 11169–11186.
6. Z. Xie, D. Tian, M. Xie, S.-Z. Yang, Y. Xu, N. Rui, J. H. Lee, S. D. Senanayake, K. Li, H. Wang, S. Kattel and J. G. Chen, *Chem*, 2020, **6**, 2703–2716.
7. Z. Xie, X. Wang, X. Chen, P. Liu and J. G. Chen, *J. Am. Chem. Soc.*, 2022, **144**, 4186-4195.
8. Z. Xie, Y. Xu, M. Xie, X. Chen, J. H. Lee, E. Stavitski, S. Kattel and J. G. Chen, *Nat. Commun.*, 2020, **11**, 1887.
9. B. Yan, S. Yao, S. Kattel, Q. Wu, Z. Xie, E. Gomez, P. Liu, D. Su and J. G. Chen, *Proc. Natl. Acad. Sci.*, 2018, **115**, 8278–8283.
10. J. Wellendorff, T. L. Silbaugh, D. Garcia-Pintos, J. K. Nørskov, T. Bligaard, F. Studt and C. T. Campbell, *Surf. Sci.*, 2015, **640**, 36-44.
11. P. Liu, *J. Chem. Phys.*, 2010, **133**, 204705-204707.
12. X. Wang, P. J. Ramírez, W. Liao, J. A. Rodriguez and P. Liu, *J. Am. Chem. Soc.*, 2021, **143**, 13103-13112.